Soft Matter

Cite this: *Soft Matter*, 2012, **8**, 1648

www.rsc.org/softmatter

PAPER

Asymmetric self-assembly of oppositely charged composite microgels and gold nanoparticles

Jérôme J. Crassous,*[a] Pierre-Eric Millard,[b] Adriana M. Mihut,[a] Frank Polzer,[c] Matthias Ballauff[d] and Peter Schurtenberger[e]

Received 25th September 2011, Accepted 16th November 2011
DOI: 10.1039/c1sm06828h

The electrostatically driven self-assembly of oppositely charged gold nanoparticles (Au NPs) and polystyrene/poly(*N*-isopropylacrylamide) (PS/PNIPAm) core-shell microgels (CSMs) has been investigated. The co-assembly was accomplished by addition of smaller Au NPs to CSMs in dilute conditions up to a number ratio of about 1 : 1, when the suspension is destabilized. A combination of different techniques (*i.e.* turbidimetric titration, electrophoretic mobility, UV-visible spectroscopy, dynamic light scattering and microscopy techniques) were used to investigate the association between the two particles and the stability of the different mixtures. Hereby we demonstrate that the size ratio between the two particles (about 4 to 1) and the asymmetric character of the association result in the formation of electrostatic hybrid complexes, analogous to dipolar colloidal molecules, which further rearrange into finite sized clusters for number ratios $N_{AuNPs}/N_{CSMs} < 1$.

1 Introduction

Colloids are well known for their analogy with dense atomic systems if we consider their phase diagram.[1] From atoms to molecules, the analogy goes further as colloidal particles can be considered as fundamental building blocks capable of mimicking molecular self-assembly through covalent and non covalent interactions.[2–4] Combining different functionalities in defined architectures would then offer numerous advantages in modern material science and soft matter-based nanotechnologies (photonic materials, biomedical diagnosis and therapy, catalysis…) and provide a better understanding of biological systems. Nevertheless while nature has succeeded in creating such systems (*e.g.*, viruses and proteins), it remains a challenge for bioinspired nanoscience to synthetically recreate these structures.

Hollow capsules, whose walls consist of colloidal particles referred to as colloidosomes[5] or photonic spheres of densely packed particles in a crystalline array[6] are some examples of assemblies from spherical colloidal particles of finite size. If the number of particles constituting the aggregate is small, the term of colloidal molecules is then employed. Many paths have been followed to design such defined clusters.[7,8] One of them consists of pickering emulsion and subsequent evaporation of the dispersed phase as shown by Pine *et al.* on micrometric polymeric particles,[9] recently extended to bidisperse colloids by Cho *et al.*[10,11] or to smaller colloidal systems by Wagner *et al.*[12] Other methods rely on templates as shown recently by Xia and coworkers[13] or follow a chemical pathway as seeded emulsion polymerization, where protrusions are grown at the surface of the seed particles.[14,15]

Particles with diversely functionalized hemispheres, so called Janus particles have also been intensively investigated[16–23] as a consequence of their self-assembly and possible applications such as stabilizers.[20,22]

Controlled aggregation between the nanoparticles in solution is another emerging field to obtain colloidal molecules.[7,8] It can either rely on the control of the electrostatic interactions,[24–26] or on the use of molecular linkers such as DNA and organic molecules.[8,27–29] An efficient separation method is then required to obtain colloidal samples with high yield of nanoparticle clusters.[8,24,26]

While well-defined colloidal geometries and functionalized particles can be achieved *via* these different methods, the next challenge is to control the range of interactions in order to direct the hierarchical assembly of these systems. Electrostatic, hydrophobic or covalent interactions can then be included. As an example Janus particles with oppositely charged hemispheres were found to reorganize into defined clusters similar to those observed *via* confinement in an emulsion.[30] The concept of

[a]*Adolphe Merkle Institute, University Fribourg, Route de l'Ancienne Papeterie, 209 1723 Marly 1, Switzerland. E-mail: jerome.crassous@unifr.ch*
[b]*Macromolecular Chemistry II, University Bayreuth, D-95440 Bayreuth, Germany*
[c]*Soft Matter and Functional Materials, Helmholtz-Zentrum Berlin für Materialien und Energie GmbH, Glienicker Strasse 100, 14109 Berlin, Germany*
[d]*Physical Chemistry I, Center for Chemistry and Chemical Engineering, Lund University, 221 00 Lund, Sweden*
[e]*Department of Physics, Humboldt University Berlin, Newtonstr. 15, 12489 Berlin, Germany*

"patches" is then usually referred to in the literature to describe particles with discrete sites of specific interactions, similar to viruses or proteins, and to predict their self-assembly. The results of different simulations illustrate the ability of patchy particles to further arrange into finite size clusters or well defined structures.[31–33]

This study aims to explore another approach to direct the self-assembly of colloidal particles based on an electrostatically driven asymmetric association between two oppositely charged colloids with a size ratio of 4 to 1. Hereby a fraction of the smaller colloids are added to the larger ones in order to generate local dipoles that will further self-assemble. The larger particles used are composite core-shell microgels (CSMs) with a polystyrene core and a crosslinked poly(*N*-isopropylacrylamide) shell. This system was used as an example of a model for the rheology of concentrated colloidal dispersions, whose choice was motivated by the tuneability of its size and interactions.[34,35] By changing the temperature, these microgels swell and deswell in a continuous or discontinuous fashion, depending on the crosslinking density with a transition from the swollen to the collapsed state taking place at the volume phase transition temperature T_{VPT} around 32 °C.[36] Not only the size of the particles can be controlled with the temperature, but also their interaction potential. Such systems synthesized by seeded emulsion polymerization with an anionic initiator were found to possess some charges originating from remaining initiator fragments. This ensures the stability of the system even after the volume phase transition.[34] Thus, the interaction potential can be adjusted by controlling the size and salt concentration of the dispersion. In an excess of salt, the system is not stable anymore above the volume phase transition and was found to reversibly coagulate.[34,37]

The smaller colloids employed for the association consisted of cationic gold nanoparticles (Au NPs). The Au NPs were synthesized following the approach proposed by Niidome *et al.*,[38] where the authors reported the application of these particles in functional gene delivery and cancerous cell detection. This system was selected because of its easy preparation, its strong contrast with respect to organic materials and the sensitivity of the optical properties of colloidal gold to the local environment,[39–43] which is of great interest when investigating the association with the core-shell microgels.

While adsorption on microgels of a large excess of small gold nanorods, silver nanoparticles[42–44] or incorporation of semiconductor nanocrystals in microgels[45] have already been reported in the past, this study now focuses on the self-assembly when composite microgels are in excess with respect to gold nanoparticles, and on the subsequent reorganization into larger structures. We proceed as follows: Au NPs were slowly added to a dilute dispersion of CSMs under turbidimetric control. Afterwards the structure and stability of the association were investigated by UV light spectroscopy, zeta potential measurement, dynamic light scattering and diverse microscopy methods.

2 Methods

Synthesis

The synthesis of PS-core particles and the polymerization of the cross-linked PNIPAm shell were performed by emulsion and seed polymerization, respectively, along lines given previously.[36,46] In this study the content of the crosslinker (*N*,*N*′)-methylenebisacrylamide (BIS) is 2.5 mol% with respect to NIPAm.

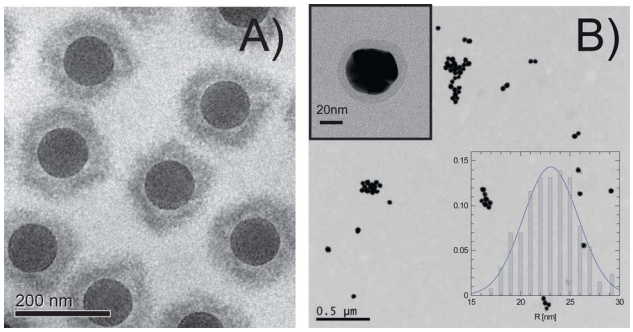

Fig. 1 A) CryoTEM micrograph of a 0.2 wt% aqueous suspension of CSMs. B) Transmission electron micrograph of a 0.2 wt% aqueous suspension of cationic Au NPs obtained by $NaBH_4$ reduction of $HAuCl_4$ in the presence of aminoethanethiol. The number distribution is reported on the histogram. The inset presents a larger magnification of a single Au NP.

Au NPs were synthesized by $NaBH_4$ reduction of $HAuCl_4$ in presence of 2-aminoethanethiol at a Au/$NaBH_4$/2-aminoethanethiol ratio of 56 : 0.1 : 85 (mol/mol/mol) following the recipe described by Niidome *et al.*[38] The particles were used for the association without further purification.

Preparation of the Au NPs-CSMs mixtures

Samples were prepared by slow addition of Au NPs suspension (0.28 g L^{-1}) onto CSMs suspension at 25 °C. The original CSMs concentration was set at 4×10^{-2} g $L^{-1}$for the samples prepared by titration, at 0.2 g L^{-1} for zeta potential and for UV light spectrometry measurement and at 0.2 g L^{-1} for the stability study. Au NPs were stable for approximately two weeks, before getting irreversibly adsorbed on the glass container surface. Thus, the characterization of the Au NPs and the preparation of the different mixtures were done with a fresh gold suspension within one week.

Measurements

Transmission electron microscopy (TEM) was performed on a Zeiss EM922 EFTEM (Zeiss NTS GmbH, Oberkochen, Germany). A few microlitres of the suspension were placed on a carbon TEM grid (Plano, 200 mesh) and the excess of liquid was removed with filter paper and the sample was left to dry before examination. The cryogenic electron microscopy (CryoTEM) was performed following the same preparation on a bare copper grid, except that the suspension was not left to dry but cryo-fixed by rapid immersion in liquid ethane as described elsewhere.[47] Scanning force microscopy (SFM) experiments were carried out on a commercial SFM (Model Dimension 3100, from Veeco Instruments Inc.). The SFM samples have been prepared by dip-coating on mica. Field-emission scanning electron microscopy (FESEM) was performed using a LEO Gemini microscope equipped with a field emission cathode. For this technique the samples have been prepared by spin coating at

2000 rpm on silicon wafers. The confocal laser-scanning microscopy (CLSM) micrographs were monitored on a Leica SP5 confocal laser-scanning microscope (CLSM) operated in the inverted mode (D6000I). The particles were non-covalently labeled with 5×10^{-3} g L^{-1} Rhodamine B (excitation at 543 nm). The suspension was prepared on a glass slide with a 200 μm spacer. The turbidity measurement and the preparation of the different Au NPs-CSMs mixtures were performed using a titrator (Titrando 809, Metrohm) equipped with a turbidity sensor ($\lambda_0 =$ 523 nm, Spectrosense, Metrohm). The UV spectra were measured by a Lambda 25 spectrometer (Perkin-Elmer), and the zeta potential was determined with the Zetasizer Nano ZS (Malvern Instruments). The same instrument was employed to determine the average hydrodynamic radius of the Au NPs measured in back scattering at 173°. Dynamic Light Scattering (DLS) measurements on the different mixtures were performed using a light scattering goniometer setup. The samples were highly diluted ($c = 2.5 \times 10^{-3}$ wt%) to prevent multiple scattering and measured for scattering angles from 30 to 130° with an increment of 10°. Measurements were carried out at 23, 33 and 45 °C. The fluctuations of the scattered light were analyzed with an ALV-5000 correlator. The measured intensity correlation functions were analyzed using the cumulant method.

3 Results and discussion

Composite microgels and gold nanoparticles

CSMs and Au NPs stabilized by aminoethanethiol were imaged, respectively, by CryoTEM (1 A) and TEM (1 B). The core-shell particles consist of a dense 51 nm radius polystyrene core, onto which a cross-linked PNIPAm shell is adsorbed (2.5 mol% cross-linking). This system has already been investigated intensively in the past by CryoTEM to directly image the volume phase transition of the PNIPAm shell at high temperatures.[47] The influence of the degree of cross-linking on the shell conformation was discussed in another study[36] and a quantitative analysis of the CryoTEM micrographs has been developed on the same system to access to the local polymer density profile of the PNIPAm shell.[48] These studies confirmed that all particles are covered with a PNIPAm shell, which is visible without using any contrast agent. The composite microgels are almost monodisperse with an overall size determined by CryoTEM, which was found to be in good agreement with the hydrodynamic radius of 113 nm measured by dynamic light scattering at room temperature.[36,48] Moreover the quantitative analysis reveals that the density profile within the microgel is not homogeneous, but parabolic in the swollen state consistent with what was reported by Stieger *et al.* for pure microgels.[49] As shown by TEM, the synthesized Au NPs are monodiperse with an average radius of 22.7 ± 3.7 nm. At higher magnification, the presence of a 5 to 8 nm thin surfactant layer on the surface of the particles could be resolved (see inset of 1 B). Thiol groups have a strong affinity to the gold surface and under neutral conditions amine groups are protonated into NH_3^+ thus generating the cationic surface charge of the particles. Moreover, the size of the corona, when compared to the size of the surfactant molecule, suggests organization into a multilayer. The overall size of the Au NPs was measured by dynamic light scattering (DLS) between 25 and 45 °C. No significant temperature dependence was observed. The average hydrodynamic radius obtained from the second cumulant analysis was found to be equal to 27 nm with a polydispersity of 0.28. We note that the DLS is more sensitive to the presence of aggregates, therefore the higher polydispersity is most probably an indication of the presence of small aggregates in the suspension and could result in an overestimation of the particle size. Taking this into account, the results of the DLS are in good agreement with the TEM analysis, particularly if we consider the contribution of the surfactant layer.

Association of Au NPs with CSMs: Turbidimetric titration

Turbidimetric titration was performed in order to follow the association of cationic Au NPs with anionic CSMs. A slow addition of CSMs to an excess of Au NPs directly led to a complete destabilization of the suspension and the formation of large aggregates. However the reverse addition of Au NPs to an excess of CSMs was found to be more stable. Therefore, the different mixtures have been prepared by slow addition of Au NPs to CSMs particles. The gold suspension (0.28 g L^{-1}) was added at a rate of 0.25 mL min^{-1} to a dilute latex suspension (16 mL) with an initial concentration of 4×10^{-2} g L^{-1}. The turbidity of the suspensions was measured during the whole addition process. The gold suspension has a strong absorption at 525 nm, which is in good agreement with the value reported by others authors for this size.[50] This value is close to the wavelength of the turbidimetric probe (523 nm). We used the transmitted intensity I_0 of the latex suspension as a reference to normalize the transmitted intensity I. Then we monitored the evolution of the absorbance defined by $A = -ln(I/I_0)$ as a function of the gold concentration, c_{AuNPs} (see Fig. 2). The absorbance increased first linearly until a critical $c_{AuNPs} = 3.0 \times 10^{-2}$ g L^{-1}, after which the absorbance increased again linearly with a lower slope. Four different samples were prepared following the same procedure (see inset of Fig. 2). In the rest of the study, we will refer to these suspensions as mix 1 for the initial CSMs suspension, and as mix 2 to 5 for the different mixtures with increasing c_{AuNPs}. At $c_{AuNPs} < 3 \times 10^{-2}$ g L^{-1}, the particles were sedimenting within a month

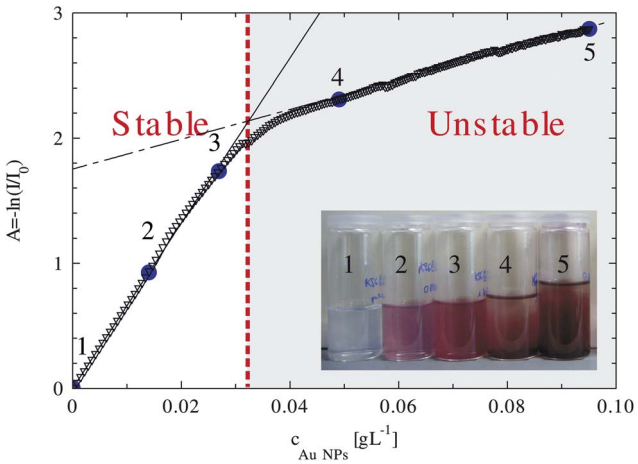

Fig. 2 Turbidimetric titration of the adsorption of Au NPs on CSMs. The numbers refer to the different mixtures presented in the inset prepared following the same procedure.

but could be fully redispersed. At higher c_{AuNPs}, the association became irreversible and the particle sedimented within one hour. Moreover some gold was absorbed on the surface of the glass container at these concentrations, which indicates the presence of free gold particles in these mixtures. We approximated the corresponding number ratio between the Au NPs and the CSMs, N_{AuNPs}/N_{CSMs}, considering the density of Au (19.3 g cm^{-3}), the size of the Au NPs determined by TEM and the number of CSMs present in suspension. At the transition between the reversible and irreversible association N_{AuNPs}/N_{CSMs} is approximately equal to 1, meaning that on average up to one Au NPs could be adsorbed on the microgels before the destabilization of the system. As it will be shown later on from the zeta potential measurements (see Fig. 7), for this critical number ratio the association maintained an overall negative charge indicating that no charge inversion occurs at the transition from the stable to unstable regime. Moreover we note that the CSMs are not subjected to any sedimentation at room temperature due to their small size, their steric stabilization ensured by the microgel and their low density. Consequently the sedimentation and/or aggregation process observed in the different mixtures already suggests the correlation of the gold with the microgels, and the formation of hybrid structures.

Thermoresponsive optical properties

We investigated the association of Au NPs with CSMs by UV-vis spectroscopy. Pure Au NPs suspension exhibits a maximum in absorption at 525 nm which is common for particles in this size range. Indeed a maximum absorption at 521 nm was found by Link *et al.*, for monodisperse 21.7 nm radius Au NPs.[50] On the contrary, the core-shell microgels did not present any specific absorption. The average number ratio N_{AuNPs}/N_{CSMs} of the three different mixtures are respectively 0.16, 0.69 and 0.93. We intentionally keep this number below the critical value of 1.05 determined from the turbidimetric titration. The three different mixtures show a red shift of the plasmon maximum from 525 to 535 nm after subtraction of the latex contribution (see inset of Fig. 3 A). Therefore no plasmon coupling takes place, which is an indication that most CSMs bear only a small number of Au NPs.

In the following step, the dependence of the absorption on the temperature was measured for a 0.2 g L^{-1} CSMs suspension with 0.12 g L^{-1} Au NPs between 10 and 45 °C (see Fig. 3 B). The absorption was found to increase with the temperature followed by a red shift from 535 to 543 nm between 10 and 45 °C. Accordingly the position of the maximum λ_{max} has been monitored for the different temperatures and compared to the variation of polymer volume fraction ϕ_p of the shell, which was reported in a former study (see Fig. 3 C).[35] The volume phase transition of the PNIPAm shell has been described using the Flory–Rehner theory as described in the same study.[35] The evolution of λ_{max} follows the same feature as the transition in the PNIPAm network, which is a good indication of the close correlation of the Au NPs with the microgel. The increase of the peak intensity and the red shift was attributed to the increase of the local refractive index upon microgel collapse as previously reported for low surface coverage by Karg *et al.* for the adsorption of gold nanorods on microgels.[42] For this purpose the effective refractive index n_{eff} of the PNIPAm shell was estimated from the polymer volume fraction ϕ_p as $n_{eff} = n_m(1 - \phi_p) + n_p\phi_p$ following the approach proposed by Weissman *et al.*[51,52] Here we use as refractive index for water $n_m = 1.33$ and for pure PNIPAm

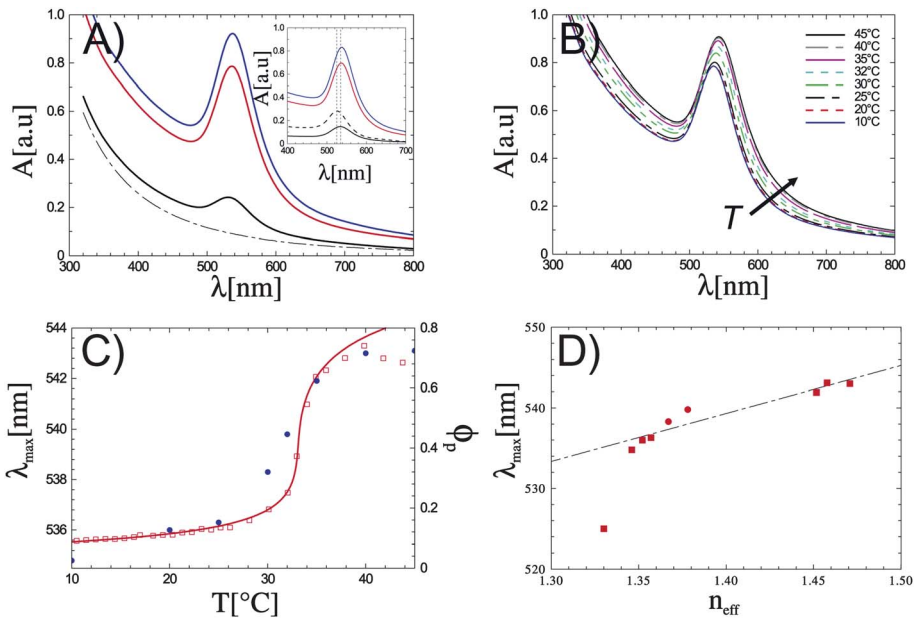

Fig. 3 A) UV-visible absorption spectra of core-shell dispersion (0.2 g L^{-1}) (dotted dashed line) and of mixtures with an increasing amount of Au NPs (0.2 g L^{-1} core-shell with $c_{AuNPs} = 0.028$, 0.12 and 0.16 g L^{-1}) measured at 20 °C. The inset displays the absorption of the pure gold (dashed line) and of the three mixtures after subtraction of the latex contribution. B) Temperature dependence of a 0.2 g L^{-1} core-shell dispersion with 0.12 g L^{-1} Au NPs. The position of the absorption maximum λ_{max} (full symbols) and the polymer volume fraction ϕ_p of the PNIPAm shell (hollow symbols) fitted by the Flory–Rehner theory (see ref. 36) are depicted as function of the temperature in (C). (D) Presents the dependence of λ_{max} as function of the effective index of refraction n_{eff}.

n_p = 1.52,[52] and neglect the dependence of the plasmon maximum position upon the temperature which should be negligible in this temperature range.[50] Fig. 3 D displays our experimental results. If we exclude the results obtained for the pure Au NPs a linear dependence of λ_{max} to n_{eff} is almost followed. The same dependence was observed in many studies for the optical properties of Au NPs in different media.[39,40,53] Nevertheless the large difference observed with the pure Au NPs most likely indicates that the particles are not fully embedded into the microgels shell but rather adsorbed at their surface.

Colloidal molecules formation and self-assembly

The different mixtures have been investigated by transmission electron microscopy (TEM) (see Fig. 4 A), scanning electron microscopy (SEM) (see Fig. 4 B) and scanning force microscopy (SFM) (see Fig. 4 C, D and E). The TEM micrograph presents a freshly prepared mix 4 (N_{AuNPs}/N_{CSMs} = 1.3). SEM and SFM were performed on mix 2 (N_{AuNPs}/N_{CSMs} = 0.93) either spin-coated on silicon wafer (SEM), or dip-coated on mica (SFM). Au NPs and CSMs could be clearly distinguished from their difference in size and contrast. The different microscopy techniques and preparation methods lead to the same result, most of the gold was adsorbed on the composite microgels and no large aggregates have been observed, except in the case of mix 4 where the suspension was unstable (N_{AuNPs}/N_{CSMs} > 1). Below the critical number ratio N_{AuNPs}/N_{CSMs} of 1 (mix 2 and 3), all the microgels are well dispersed on the different wafers independently of the sample preparation. The adsorption was not uniform. Indeed free CSMs could be observed, whereas some of them bear up to three Au NPs. Fig. 4 D considers a single CSM–Au NP dipole. The PNIPAm shell adsorbed on the wafer could be clearly imaged by the SFM phase micrograph. The Au NP appears strongly correlated to the CSM as can be seen from the PNIPAm shell deformation. Dashed lines indicate the radius of the polystyrene core determined by TEM, and the radii of the CSMs and of the Au NPs measured by DLS. The dimensions determined by this method provide here a good estimation of the size of the different components observed by SFM.

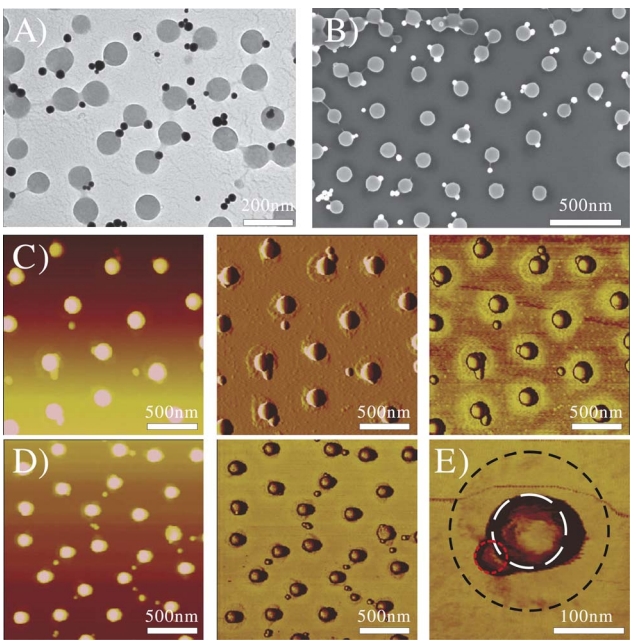

Fig. 4 A) TEM micrographs of the mix 4. B) SEM micrographs of the mix 3. C) SFM micrographs of the mix 3 (left: height, middle: amplitude, right: phase). D) SFM micrographs of the mix 2 (left: height, right: phase). E) Phase contrast of a single dipole. The long dashed line refers to the average radius of the core particles equal to 52 nm as determined by electron microscopy. The short dashed line gives the hydrodynamic radius of the pure core-shell particles determined by DLS at 23 °C (= 113 nm) and the dotted line the average radius of the Au NPs determined by TEM (= 22.7 nm).

As described previously, our former experiments clearly indicated the association between the Au NPs and the CSMs. Moreover the microscopic examination of the sample established the presence of separated hybrid complexes consisting of a CSM bearing one to three Au NPs if N_{AuNPs}/N_{CSMs} < 1. As this association consists of oppositely charged particles, we will now further investigate the structure and self-assembly of these complexes in suspension. DLS (Fig. 5) was performed on mix 1, 2 and 3 at 23, 33 and 45 °C. Mix 1 refers to pure CSMs, whereas mix 2 and mix 3 correspond to N_{AuNPs}/N_{CSMs} respectively equal to 0.47 and 0.93. Addition of AuNPs was followed by a slowing down of the dynamics as shown on the autocorrelation functions, where the decorrelation shifts to longer times (Fig. 5 A) consecutive to a rearrangement in suspension into larger structures. The average decay rate Γ was determined from the second cumulant analysis of the autocorrelation function measured for scattering angles varying from 30 to 130° with an increment of 10°. The diffusion coefficient D was derived from the linear dependence $\Gamma = Dq^2$, where **q** is the scattering vector. A linear dependence of Γ *versus* q^2 was observed for the full **q**-range for all

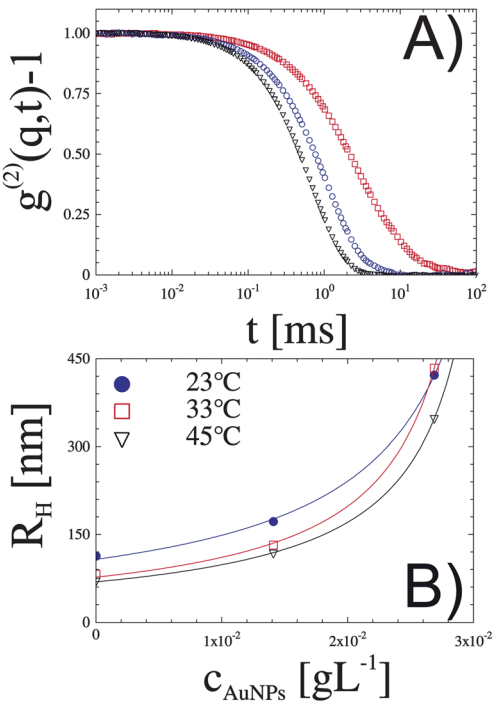

Fig. 5 A) Intensity autocorrelation function measured at 23 °C on mix 1 (down triangles), mix 2 (circles) and mix 3 (squares). B) Apparent hydrodynamic radii obtained from the linear extrapolation as function of the gold concentration at 23 °C (full circles), 33 °C (squares) and 45 °C (down triangles). Lines are here to guide the eyes.

the mixtures at the three different temperatures. The different results are summarized in Fig. 5 B where the average hydrodynamic radius R_H obtained from D using the Stokes–Einstein relation is considered as function of c_{AuNPs} for different temperatures. At 23 °C, addition of Au NPs resulted in an increase of the hydrodynamic radius from 113 (pure CSMs) to 172 (mix 2) and 422 nm (mix 3). In all cases the apparent hydrodynamic radii of the two mixtures are larger than what could be expected for a single dipole. Furthermore the average polydispersity derived from this analysis was found to increase from 0.07 for the pure CSMs to 0.46 for the mix 2 and 0.86 for mix 3 as we approach the critical number ratio $N_{AuNPs}/N_{CSMs} = 1$, above which the particles irreversibly aggregate. Similar to pure CSMs, these clusters are also responding to the temperature. Indeed the average apparent radius was found to decrease between 20 and 45 °C from 172 to 118 nm (mix 2), and from 422 to 345 nm (mix 3).

The formation of clusters was then directly imaged by confocal laser-scanning microscopy (CLSM) (see Fig. 6). For this purpose mix 1, 2 and 3 ($N_{AuNPs}/N_{CSMs} = 0$, 0.47 and 0.93) were stained by addition of water soluble Rhodamine B (5×10^{-3} g L^{-1}). After preparation of the sample, most of the particles adsorbed on the cover slide. No particles could be resolved in suspension considering the high dilution and the fast dynamics of the different objects. Therefore we only imaged particles and/or complexes adsorbed at the surface of the cover slide. In respect to micrographs without addition of Au NPs, where no clear structure formation could be observed (Fig. 6 A and D), the association of the CSMs with the Au NPs appears in the form of well-defined spherical clusters (see Fig. 6 B, C, E and F). In good agreement with DLS analysis, the proportion and size of the clusters was found to increase with the addition of Au NPs. As a comparison the hydrodynamic radii determined at 23 °C for the different mixtures are indicated by the dashed circles. The two techniques are in good agreement considering the different sensitivity of the methods. The overall size, much larger than the radii of a single dipole, confirms the reorganization of the dipoles into defined clusters.

As evidenced by microscopy methods in the dried state, the addition of a reduced number of Au NPs thus results in the formation of colloidal molecules consisting of a CSM bearing Au NPs. Driven by the dipolar character of the association, such colloidal molecules then further self-assemble into finite size clusters, of which the size and/or proportion in the suspension increase with increasing c_{AuNPs} as shown by DLS and CLSM. In the following sections, we will address the question of their stability as function of the temperature.

Zeta potential of the clusters

The temperature dependence of the zeta potential of polystyrene core, CSM and Au NP has been measured between 20 and 50 °C (see Fig. 7). The measured zeta potential of the Au NPs was not sensitive to the temperature and its average value was found equal to +27 mV confirming the cationic character of the particles. Similarly, the zeta potential of polystyrene core particles was found to be constant (≈ -43 mV) over the whole temperature range. Below T_{VPT}, in the swollen state, the CSMs zeta potential was found around −15 mV, reflecting both low charge density and high friction coefficient of the particles. A dramatic change in zeta potential was observed above T_{VPT} when the NIPAm shell collapsed. As expected, the absolute values of the zeta potential increased with the temperature to reach approximately the value of the core. As described in other studies,[54,55] the temperature dependence of the zeta potential could be interpreted by the increase in the charge density due to the reduction of the particle size and by the reduction of the frictional coefficient as the softness decreases with the collapse of the NIPAm network. This last effect could be directly visualized by Cryo-TEM, where the particles present a fuzzy shell below the VPT temperature with a transition to a collapsed and dense state at higher temperature.[47] Different mixtures consisting of 0.2 g L^{-1}

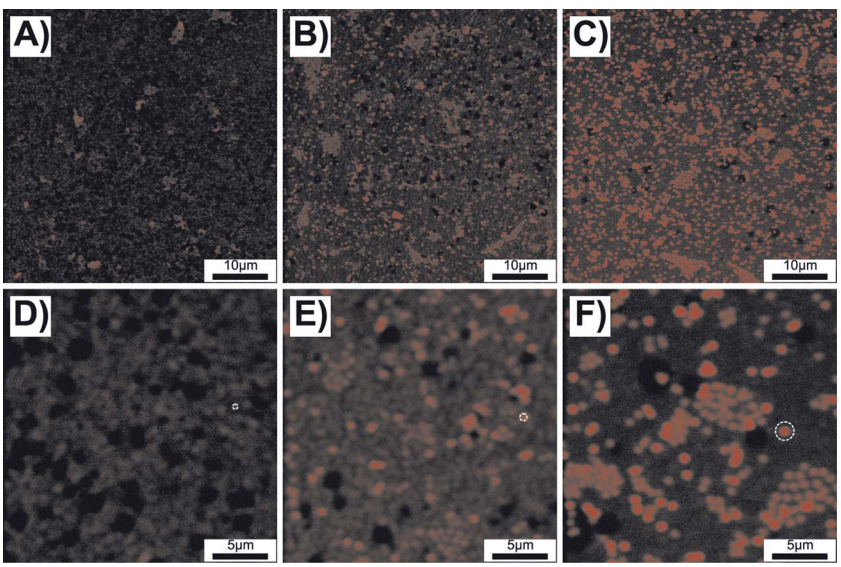

Fig. 6 Confocal micrographs of the association between the Au NPs and the composite microgels of the mix 1 (A, D), 2 (B, E) and 3 (C, F) measured at 23 °C. The dashed circles refer to the estimation of the overall size determined by dynamic light scattering.

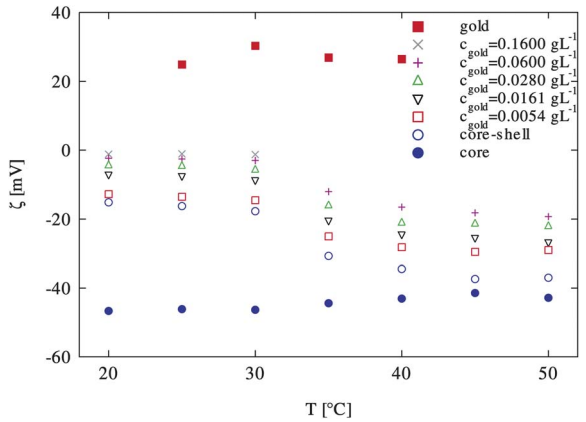

Fig. 7 Temperature dependent zeta potential measurements for the Au NPs, the PS core, the PS/PNIPAm core-shell particles and their mixture with different Au NPs content as indicated in the legend (see text for further details).

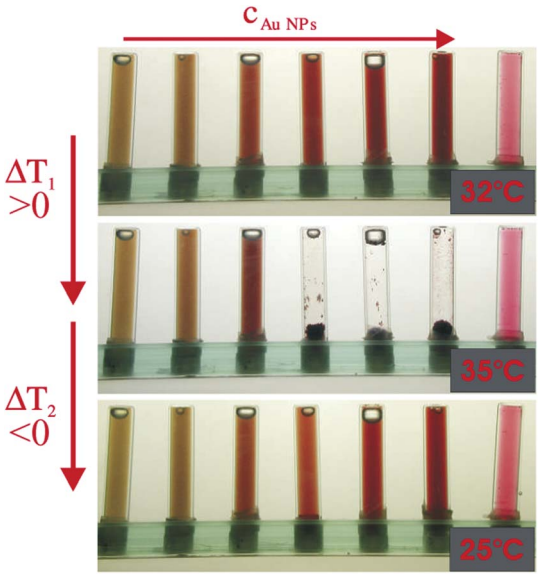

Fig. 8 Temperature dependent stability of Au NPs-CSMs suspensions as function of the concentration of the Au NPs suspension in the mixture. The composition of the different mixtures are from the right to the left: $c_{CSMs} = 2$ g L^{-1}) with $c_{AuNPs} = 0$, 0.054, 0.107, 0.160, 0.220, 0.280 g L^{-1} and a pure 0.2 g L^{-1} Au NPs suspension. All suspensions were first heated at 32 °C, then at 35 °C and afterwards cooled down at 25 °C.

CSMs with c_{AuNPs} varying between 5.4×10^{-3} g L^{-1} ($N_{AuNPs}/N_{CSMs} = 0.32$) and 1.6×10^{-1} g L^{-1} ($N_{AuNPs}/N_{CSMs} = 0.96$) were measured. The CSMs concentration was about 5 times higher than the mixtures investigated in the former section for the turbidimetric titration whereas the number of Au NPs per CSM was maintained below the critical value of 1. Below 32 °C, the absolute value of the zeta potential decreases upon addition of Au NPs to almost zero for a concentration of 1.6×10^{-1} g L^{-1}. At higher temperatures, the thermosensitivity was maintained with a transition around T_{VPT} of the pure CSMs. For $c_{AuNPs} \geq 1.6.10^{-1}$ g L^{-1} a coagulation process has been observed above 40 °C. The decrease of the absolute value of the zeta potential could be interpreted as a consequence of the cluster formation, resulting in an increase of the size and a decrease of the overall charge. Moreover the concentration of Au NPs in suspension also directs the concentration of free cationic surfactant. This last parameter is crucial for the stability of the suspension as it screened the electrostatic interactions.

Colloidal stability and thermoreversible coagulation

The stability of the suspensions as function of temperature and Au NPs concentration was determined for different mixtures (see Fig. 8). In order to investigate the effect of the free surfactant, the concentration of the composite microgel in this case was much higher (2 g L^{-1}) and the Au NPs concentration was varied between 0.054 up to 0.28 g L^{-1}, corresponding to N_{AuNPs}/N_{CSMs} far below 1 (from 0.03 to 0.17). Whereas the different mixtures were fully stable below T_{VPT}, increasing the temperature to 35 °C results in the coagulation of the system for $c_{AuNPs} \geq 0.16$ g L^{-1}. After sedimentation of the coagulates, we observed from the clear supernatant that most of the Au NPs had complexed the microgels. By cooling down the suspensions to 25 °C the different mixtures could be fully redispersed, demonstrating the reversibility of the coagulation process, similar to what has been observed after addition of an excess of salt on pure core-shell dispersions.[34] Note that this behavior is different to what was observed for N_{AuNPs}/N_{CSMs} higher than 1, where coagulation/sedimentation is totally irreversible. The CSMs are sterically stabilized by the PNIPAm shell and electrostatically due to the use during their synthesis of anionic initiator and surfactant. Addition of salt, or of an oppositely charged surfactant reduces the range of the electrostatic interactions. Above T_{VPT}, the steric stabilization vanished as the microgels collapses. If the ionic strength related to the concentration of free surfactant is too high, the screened electrostatic interactions are not able to maintain the stability of the suspension and the system coagulates. In order to determine the influence of the free surfactant present in suspension, the same experiment was repeated after a dilution of the different mixtures by a factor of ten. No coagulation was observed under these conditions. Nevertheless the former experiments have shown that if $c_{AuNPs} \geq 0.160$ g L^{-1} the system coagulates for latex concentrations of 2 and 0.2 g L^{-1}. Therefore we conclude that the Au NPs suspension concentration, directly related to the free surfactant concentration, and not the number ratio Au NPs/CSMs is responsible for the thermoreversible coagulation at high temperatures.

Control of the colloidal self-assembly

Fig. 9 summarizes the association process between cationic gold nanoparticles (Au NPs) and anionic core-shell microgels (CSMs) as a function of temperature, number ratio N_{AuNPs}/N_{CSMs} and Au NPs concentration. The originality of the association is ensured by the CSMs particles, which are electrosterically stabilized by the large crosslinked PNIPAm shell and the residual charges originating from the anionic initiator and the remaining SDS surfactant. These charges present at the surface of the polystyrene core and dispersed into the fuzzy microgel shell ensure the stability of the CSMs at high temperatures when the ionic strength is low. Colloidal molecules in the form of defined

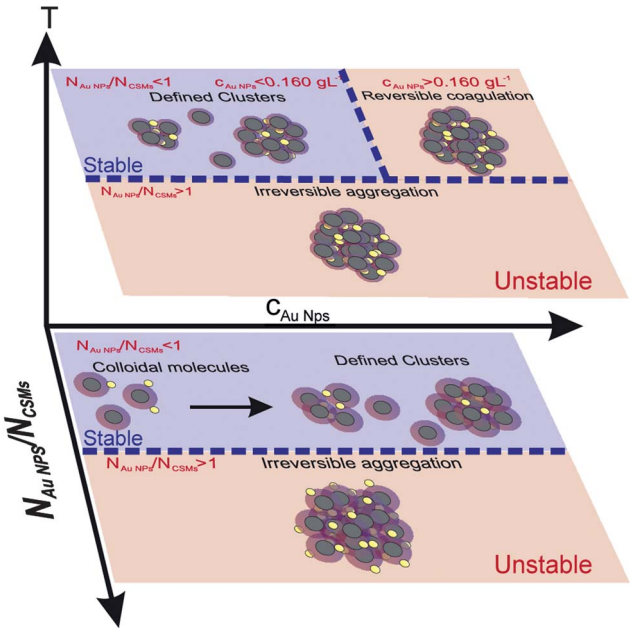

Fig. 9 Schematic representation of the association process: colloidal molecules formed by the adsorption of the cationic Au NPs with the anionic CSMs rearranged in suspension into defined sized clusters when $N_{AuNPs}/N_{CSMs} < 1$. At higher number ratio the suspension becomes unstable and irreversibly aggregates. When the temperature increases the PNIPAm shell of the CSMs collapses and defined clusters are obtained as long as $c_{AuNPs} \geq 0.160$ g L^{-1}. Above this critical concentration, the screened hybrid complexes reversibly coagulate for temperatures exceeding the VPT temperature of the CSMs.

hybrid complexes consisting of CSMs bearing 1 to 3 Au NPs could be obtained in an asymmetric association between oppositely charged Au NPs and CSMs, when only a few Au NPs are adsorbed at the surface of the CSMs. When the number ratio $N_{AuNPs}/N_{CSMs} \leq 1$, these colloidal molecules further reorganize with free CSMs and other colloidal molecules present in the suspension into stable defined clusters. The defined clusters were sensitive to the temperature, at low N_{AuNPs}/N_{CSMs} the apparent size was found to decrease above the VPT of the CSMs. In an excess of Au NPs, when $N_{AuNPs}/N_{CSMs} > 1$, the suspensions becomes unstable and irreversibly aggregate. The free surfactant present in the Au NPs suspension controls the range of the interactions and the stability above the volume phase transition temperature T_{VPT} of the NIPAm network. As a consequence, for $N_{AuNPs}/N_{CSMs} < 1$ and $c_{AuNPs} > 0.160$ g L^{-1} the excess of free surfactant screened the electrostatic stabilization and the suspensions were found to thermoreversibly coagulate above T_{VPT} of the CSMs.

4 Conclusion

We investigated the asymmetric association of oppositely charged gold nanoparticles (Au NPs) and composite core-shell microgels (CSMs) polystyrene/poly(*N*-isopropylacrylamide) (PS/NIPAm). Our approach demonstrated that the controlled adsorption of a reduced number of Au NPs at the surface of the CSMs generates colloidal molecules composed of single CSMs bearing one to three Au NPs. The dipolar character of such colloidal molecules drive them to further rearrange into finite size clusters. Similar to colloidal Janus dipoles or to patchy particles used in computer simulations, which could rearrange into defined structures, the prerequisite for a stable cluster formation is the presence of a single small patch and short range interactions. The small patch was ensured by the size ratio Au NPs/CSMs of about 1 to 4, whereas the range of interaction was adjusted with the temperature and the ionic strength related to the presence of free surfactant. In this way the size of the clusters was found to vary with the number ratio, which defined the number of patches and therefore the valence of the colloidal molecules. Moreover, the presence of the microgels implements the additional sensitivity to the temperature in such way that the size and stability of the clusters could be controlled with the temperature. Indeed in the screened electrostatic regime, we demonstrated that the clusters thermoreversibly coagulate above the volume phase transition temperature of the NIPAm network.

These first experiments open a new fascinating research field, where microgels are particularly appealing in respect to their high stability below the VPT and to their interaction potential that can be adjusted from soft repulsive to attractive as a function of the temperature and the ionic strength. They represent the perfect candidates to investigate colloidal self-assembly, and to improve our understanding of complex biological mixtures where the difference of sizes and the balance of the interactions is driving the association process.

Acknowledgements

We acknowledge financial support by the Deutsche Forschungsgemeinschaft, SFB 481, Bayreuth, the Adolphe Merkle foundation and the Swiss National Foundation. The authors are indebted to Benjamin Goßler for the SEM and Markus Drechsler for his contribution in the CryoTEM microscopy.

References

1 V. J. Anderson and H. N. W. Lekkerkerker, *Nature*, 2002, **416**, 811.
2 S. C. Glotzer, M. J. Solomon and N. A. Kotov, *AIChE J.*, 2004, **50**, 2978.
3 E. W. Edwards, D. Wang and H. Mohwald, *Macromol. Chem. Phys.*, 2007, **208**, 439.
4 A. B. Pawar and I. Kretzschmar, *Macromol. Rapid Commun.*, 2010, **31**, 150.
5 A. D. Dinsmore, M. F. Hsu, M. G. Nikolaides, M. Marquez, A. R. Bausch and D. A. Weitz, *Science*, 2002, **298**, 1006.
6 J. H. Moon, G. R. Yi, S. M. Yang, D. J. Pine and S. B. Park, *Adv. Mater.*, 2004, **16**, 605.
7 D. Velegol, H. A. Jerri, J. J. McDermott and N. Chaturvedi, *AIChE*, 2010, **56**, 564.
8 J. M. Romo-Herrera, R. A. Alvarez-Puebla and L. M. Liz-Marzan, *Nanoscale*, 2011, **3**, 1304.
9 V. N. Manoharan, M. T. Elsesser and D. J. Pine, *Science*, 2003, **301**, 483.
10 Y. S. Cho, G. R. Yi, J. M. Lim, S. H. Kim, V. N. Manoraharan, D. J. Pine and S. M. Yang, *J. Am. Chem. Soc.*, 2005, **127**, 15968.
11 Y. S. Cho, G. R. Yi, S. H. Kim, S. J. Jeon, M. T. Elsesser, H. K. Yu, S. M. Yang and D. J. Pine, *Chem. Mater.*, 2007, **19**, 3183.
12 C. N. Wagner and A. Wittemann, *Langmuir*, 2008, **4**, 12126.
13 Y. N. Xia, Y. D. Yin, Y. Lu and J. McLellan, *Adv. Funct. Mater.*, 2003, **13**, 907.
14 S. Reculusa, C. Poncet-Legrand, S. Ravaine, C. Mingotaud, E. Duguet and E. Bourgeat-Lami, *Chem. Mater.*, 2002, **14**, 2354.
15 S. Reculusa, C. Mingotaud, E. Bourgeat-Lami, E. Duguet and S. Ravaine, *Nano Lett.*, 2004, **4**, 1677.

16 A. Perro, S. Reculusa, S. Ravaine, E. Bourgeat-Lamic and E. Duguet, *J. Mater. Chem.*, 2005, **15**, 3745.
17 S. Berger, A. Synytska, L. Ionov, K. J. Eichhorn and M. Stamm, *Macromolecules*, 2008, **41**, 9669.
18 W. Lu, M. Chen and L. Wu, *J. Colloid Interface Sci.*, 2008, **328**, 98.
19 T. Isojima, M. Lattuada, J. B. V. Sande and T. A. Hatton, *ACS Nano*, 2008, **2**, 1799.
20 J. W. Kim, D. Lee, H. C. Shum and D. A. Weitz, *Adv. Mater.*, 2008, **20**, 3239.
21 B. B. Wang, B. Li, B. Zhao and C. Y. Li, *J. Am. Chem. Soc.*, 2008, **130**, 11594.
22 A. Walther and A. H. E. Müller, *Soft Matter*, 2008, **4**, 663.
23 M. Hoffmann, Y. Lu, M. Schrinner and M. Ballauff, *J. Phys. Chem. B*, 2008, **112**, 14843.
24 P. M. Johnson, C. M. van Kats and A. van Blaaderen, *Langmuir*, 2005, **21**, 11510.
25 A. M. Yake, R. A. Panella, C. E. Snyder and D. Velegol, *Langmuir*, 2006, **22**, 9135.
26 G. Chen, Y. Wang, L. H. Tan, M. X. Yang, L. S. Tan, Y. Chen and H. Y. Chen, *J. Am. Chem. Soc.*, 2009, **131**, 4218–4219.
27 A. P. Alivisatos, K. P. Johnsson, X. G. Peng, T. E. Wilson, C. J. Loweth, M. P. Bruchez and P. G. Schultz, *Nature*, 1996, **382**, 609–611.
28 A. L. Hiddessen, S. D. Rodgers, D. A. Weitz and D. A. Hammer, *Langmuir*, 2000, **16**, 9744.
29 D. Zanchet, C. M. Micheel, W. J. Parak, D. Gerion, S. C. Williams and A. P. Alivisatos, *J. Phys. Chem. B*, 2002, **106**, 11758–11763.
30 L. Hong, A. Cacciuto, E. Luijten and S. Granick, *Nano Lett.*, 2006, **6**, 2510.
31 Z. Zhang and S. C. Glotzer, *Nano Lett.*, 2004, **4**, 1407.
32 A. Giacometti, F. Lado, J. Largo, G. Pastore and F. Sciortino, *J. Chem. Phys.*, 2010, **132**, 174110.
33 F. Sciortino, A. Giacometti and G. Pastorec, *Phys. Chem. Chem. Phys.*, 2010, **12**, 11869.
34 J. J. Crassous, M. Siebenbuerger, M. Ballauff, M. Drechsler, O. Henrich and M. Fuchs, *J. Chem. Phys.*, 2006, **125**, 204906.
35 J. J. Crassous, M. Siebenbuerger, M. Ballauff, M. Drechsler, D. Hajnal, O. Henrich and M. Fuchs, *J. Chem. Phys.*, 2008, **128**, 204902.
36 J. J. Crassous, A. Wittemann, M. Siebenbuerger, M. Schrinner, M. Drechsler and M. Ballauff, *Colloid Polym. Sci.*, 2008, **286**, 805.
37 A. Zaccone, J. J. Crassous, B. Béri and M. Ballauff, *Phys. Rev. Lett.*, 2011, **107**, 168303.
38 T. Niidome, K. Nakashima, H. Takashi and Y. Niidome, *Chem. Commun.*, 2004, **17**, 1978.
39 P. Hanarp, M. Kall and D. S. Sutherland, *J. Phys. Chem. B*, 2003, **107**, 5768.
40 A. J. Haes, S. L. Zou, G. C. Schatz and R. P. J. V. Duyne, *J. Phys. Chem. B*, 2004, **108**, 6961.
41 M. Rasmusson, A. Routh and B. Vincent, *Langmuir*, 2004, **20**, 3536.
42 M. Karg, I. Pastoriza-Santos, J. Perez-Juste, T. Hellweg, L. M. Liz-Marzan and M. Luis, *Small*, 2007, **3**, 1222.
43 M. Das, N. Sanson, D. Fava and E. Kumacheva, *Langmuir*, 2007, **23**, 196.
44 Q. Sun and Y. Deng, *Langmuir*, 2005, **21**, 5812.
45 M. Kuang, D. Y. Wang, H. B. Bao, M. Y. Gao, H. Mohwald and M. Jiang, *Adv. Mater.*, 2005, **17**, 267.
46 N. Dingenouts, C. Norhausen and M. Ballauff, *Macromolecules*, 1998, **31**, 8912.
47 J. J. Crassous, M. Ballauff, M. Drechsler, J. Schmidt and Y. Talmon, *Langmuir*, 2006, **22**, 2403.
48 J. J. Crassous, C. N. Rochette, A. Wittemann, M. Schrinner and M. Ballauff, *Langmuir*, 2009, **25**, 7862.
49 M. Stieger, W. Richtering, J. S. Pedersen and P. Linder, *J. Chem. Phys.*, 2004, **120**, 6197.
50 S. Link and M. A. El-Sayed, *J. Phys. Chem. B*, 1999, **103**, 4212.
51 J. M. Weissman, H. B. Sunkara, A. S. Tse and S. A. Asher, *Science*, 1996, **274**, 959.
52 M. Reufer, P. Daz-Leyva, I. Lynch and F. Scheffold, *Eur. Phys. J. E*, 2009, **28**, 165.
53 G. Raschke, S. Brogl, A. S. Susha, A. L. Rogach, T. A. Klar, J. Feldmann, B. Fieres, N. Petkov, T. Bein, A. Nichtl and K. Kurzinger, *Nano Lett.*, 2004, **4**, 1853.
54 K. Makino, S. Yamamoto, K. Fujimoto, H. Kawaguchi and H. Oshima, *J. Colloid Interface Sci.*, 1994, **166**, 251.
55 T. López-León, J. L. Ortega-Vinuesa, D. Bastos-Gonzalez and A. Elaïssari, *J. Phys. Chem. B*, 2006, **110**, 4629.

